# A detailed modeling of thermoelectric generator for maximum power point tracking

1 author:

Hayati Mamur
Manisa Celal Bayar University, Manisa, TURKEY

**57** PUBLICATIONS  **418** CITATIONS

SEE PROFILE

Some of the authors of this publication are also working on these related projects:

1. Design of grid off convertor and invertor system for a micro wind turbine of 1 kW View project

PID Parameter Optimization of Blade Pitch Controller in Wind Turbines by a New Intelligent Genetic Algorithm Article Control of Pitch Angle of Wind Turbine by Fuzzy Pid Controller View project

# Detailed modeling of a thermoelectric generator for maximum power point tracking

**Hayati MAMUR**[1,]*[⊙], **Yusuf ÇOBAN**[2][⊙]
[1]Department of Electrical and Electronics Engineering, Faculty of Engineering,
Manisa Celal Bayar University, Manisa, Turkey
[2]Air NCO Higher Vocational School, National Defense University, İzmir, Turkey

**Abstract:** Thermoelectric generators (TEGs) are used in small power applications to generate electrical energy from waste heats. Maximum power is obtained when the connected load to the ends of TEGs matches their internal resistance. However, impedance matching cannot always be ensured. Therefore, TEGs operate at lower efficiency. For this reason, maximum power point tracking (MPPT) algorithms are utilized. In this study, both TEGs and a boost converter with MPPT were modeled together. Detailed modeling, simulation, and verification of TEGs depending on the Seebeck coefficient, the hot/cold side temperatures, and the number of modules in MATLAB/Simulink were carried out. In addition, a boost converter having a perturb and observation (P&O) MPPT algorithm was added to the TEG modeling. After the TEG output equations were determined, the TEG modeling was performed based on manufacturer data sheets. Thanks to the TEG model and the boost converter with P&O MPPT, the maximum power was tracked with a value of 98.64% and the power derived from the TEG was nearly unaffected by the load changes. The power outputs obtained from the system with and without MPPT were compared to emphasize the importance of MPPT. These simulation values were verified by using an experimental setup. Ultimately, the proposed modeling provides a system of TEGs and a boost converter having P&O MPPT.

**Key words:** Thermoelectric generator, modeling, MPPT, MATLAB/Simulink

## 1. Introduction

Thermoelectric generators (TEGs) are semiconductor devices that convert the temperature difference between surfaces into electrical energy directly [1]. In order to increase their voltage, thermoelements (TEs) of $p$ and $n$ types are electrically connected in series and thermally connected in parallel to raise thermal conductivity [2]. They are utilized as small power electric energy sources both to gain electrical energy from waste heats and to contribute to energy efficiency [3–6].

TEGs have some advantages and disadvantages. Their advantages are that there are no moving parts, they have a long service life, and they operate quietly. Moreover, they do not release greenhouse gases and therefore do not have any harmful effects on the environment. However, they have two disadvantages, which are low efficiency and high cost. For these reasons, the usage areas are limited [7, 8]. However, considering the contribution of TEGs to energy efficiency, the generated electricity is quite valuable.

When a load is directly connected to TEG terminals, if the load resistance and the internal resistance of the TEG are not equal, TEG efficiency decreases further. This is called an impedance imbalance [9–11]. In

---

*Correspondence: hayati.mamur@cbu.edu.tr

order to avoid this, they are used with converters that perform both maximum power point tracking (MPPT) and power regulation as in photovoltaic panels (PVs) [12–15]. Various algorithms have been developed for the MPPT process in these converters. It is observed that these algorithms are adapted from PVs [16, 17]. The most common of these is the perturb and observation (P&O) algorithm. The algorithm is a reference for other algorithms and the results of the developed algorithms are compared with those of the algorithm [18, 19]. The focus of the present study is on detailed modeling of a TEG with the Seebeck coefficient and temperature difference provided by the TEG manufacturers, as well as the minimization of impedance imbalance by means of a boost converter with P&O MPPT.

TEG manufacturers publish datasheets of TEGs. The datasheets include maximum power, current, and voltage when the impedance matching is provided. Furthermore, they ensure hot and cold surface temperatures that can be reached by TEGs. In addition, they indicate the Seebeck coefficient, which is one of the most important criteria. When a TEG is modeled via temperature difference and Seebeck coefficient, the power value taken from the TEG can be calculated easily. Furthermore, the power of TEGs is low. For this reason, they must be connected in series and parallel to achieve the desired power value [20, 21]. They are connected in series in order to increase voltage and connected in parallel in order to raise current. If the numbers of series and parallel connected TEGs are arranged in modeling, ideal modeling will be carried out for industrial TEG users.

In the literature, TEG models have been given with the product characteristics of the manufacturers. In these studies, hot and cold side temperatures, power, voltage, and current matching and optimal efficiency values were used together for the TEG models [22]. The responses of TEGs were measured by observing the changes in rapidly changing temperature conditions [23]. Moreover, the efficiency values obtained from the series/parallel connection of TEGs with each other were determined [24]. In addition, TEGs have been utilized in both thermoelectric coolers (TECs) and PVs to improve energy efficiency in grid-on and grid-off applications [25, 26]. They contribute to increase the energy efficiency of PV panels throughout by converting the temperature difference between the heated and the relatively cold surfaces of PV into electrical energy.

When the modeling studies are examined carefully, the detailed modelings of PV by MATLAB/Simulink are quite common and these are the basis of other studies [27–33]. However, it appears that TEGs have not been modeled in detail by means of Seebeck coefficient and cold-hot side temperature values. Therefore, the present study is based on the modeling of TEGs with these parameters so that MPPT applications can be implemented easily via SimPowerSystems in MATLAB/Simulink. Additionally, the present study provides boost converter modeling with a P&O MPPT algorithm. Finally, the results of TEG modeling with and without MPPT have been compared and confirmed by means of an experimental liquid–liquid TEG system setup newly installed.

One of the most important features of the present paper, which differs from the studies in the literature, is to simulate TEGs by entering the Seebeck coefficient, the hot/cold side temperatures, and the number of modules, as well as the addition of MPPT to these simulation studies. There are some models in the literature related to TEGs [9, 10, 22]. However, when these studies are taken into consideration, it is seen that there is no study involving comprehensive modeling. TEG modeling, boost converter modeling with and without P&O MPPT, and the verification of these simulation studies by means of an experimental setup will be a great source for researchers in this field.

The presentation of the present study is as follows. After giving the introduction section in the first part of the study, the TEG structure, equations, characteristic curves, a boost converter, and a P&O MPPT algorithm are expressed in the material section. The third section is divided into three parts. One of them

is TEG modeling carried out by means of the hot/cold side temperatures and Seebeck coefficient. Second is series/parallel connected TEG modeling and the last one is TEG modeling with a boost converter having P&O MPPT. Then, in the fourth section, the modeling and the experimental outcomes and discussions are given. Finally, the results are explained at the end of the study.

## 2. Material

In this section, the structure, equations, and characteristic curves of TEGs, a boost converter, and a P&O MPPT algorithm are expressed.

### 2.1. TEGs

A TE is formed by combining high figure of merit $p$ and $n$ type semiconductors. The TEs are connected in series with each other to increase the voltage. TEGs are made up by connecting the TEs in parallel with the help of ceramic plates in order to raise thermal conductivity. When a temperature difference between the ceramic plates is generated, heat transfer from the hot surface to the cold surface becomes possible. The heat transfer leads to electron flow from the $n$-type to the $p$-type semiconductors. Thus, a voltage is generated as follows:

$$V_{OC} = \alpha . \Delta T, \tag{1}$$

where $V_{OC}$ is the open circuit voltage (V) of the TEG, $\alpha$ is the Seebeck coefficient (V/K), and $\Delta T$ is the temperature difference (K). The temperature difference is between the hot, $T_h$, and the cold surfaces, $T_c$, ($\Delta T = T_h - T_c$). The Seebeck coefficient of a good material varies between 100 and 300 $\mu$V/K. The temperature value is determined according to the catalog information provided by manufacturers. The TEGs used for industrial purposes have a hot surface temperature of up to $350°$C. The value is higher in TEGs used in vehicle exhaust systems.

The electrical equivalent circuit of a TEG consists of a temperature-dependent voltage source and an internal resistor, $R_{in}$. A load, $R_L$, is connected to the TEG for generating power. When the load value and the internal resistance of the TEG match ($R_{in} = R_L$), the power generated from the TEG reaches a maximum power point (MPP). As the load value changes, the generated power decreases. When the load is infinite, an open-circuit voltage is measured from the TEG terminals. Similarly, the load is zero when TEG terminals are shorted. Therefore, a short-circuit current passes through the TEG. When the power taken from a TEG is at the MPP point, the open-circuit voltage and the short-circuit current are also in their half-value as described below:

$$V_{MPP} = V_{OC}/2 \tag{2}$$

$$I_{MPP} = I_{SC}/2, \tag{3}$$

where $V_{MPP}$ and $I_{MPP}$ are the voltage (V) and the current (A) at the MPP, respectively. $I_{SC}$ is the short-circuit current (A). The MPP can be defined with these values.

The value of the current passing through the TEG is given below:

$$I_{TEG} = V_{OC}/(R_{int} + R_L), \tag{4}$$

where $I_{TEG}$, $R_{int}$, and $R_L$ are the current of TEG (A), the internal resistance of TEG ($\Omega$), and the load resistance ($\Omega$), respectively.

Depending on the load resistance and the internal resistance, the power taken from the TEG is as follows:

$$P = V_{OC}^2 . R_L / (R_{int} + R_L)^2, \tag{5}$$

where $P$ is the power generated from the TEG (W). The power is sensitive to load changes; at the same time, it is directly proportional to the temperature difference. As the temperature difference is raised, the power value also increases and, as a result, the MPP changes. If an equal and constant load to the internal resistance of the TEG is connected, the MPP value can be captured for a given temperature difference. However, as the temperature difference varies, the MPP shifts from the old MPP. The load must be adaptive so that the MPP value can be tracked continuously. For this purpose, an adaptation circuit is placed between the TEG and the load. The circuits are converters performing both power regulation and MPPT.

## 2.2. Boost converter

DC–DC converters are electronic devices that efficiently change the voltage level from one value to another. They are in the group of not insulated converters that increase the DC voltage level from low to high. A boost converter is illustrated in Figure 1a. The coil of the converter is very important for MPPs. The MPP points are captured by programmable coil current. This is the principle of MPPT, as presented in Figure 1b. The block diagram of a TEG system with MPPT is also presented in Figure 1c.



(a)    (b)    (c)
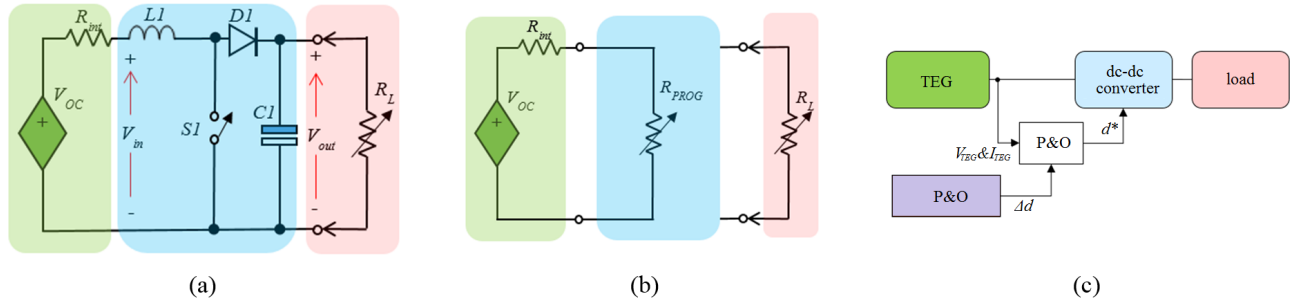
**Figure 1**. For MPPT (a) boost converter, (b) MPPT principle, and (c) block diagram.

The voltage in a boost converter is raised by switching the S1 switch from a few kHz to a few MHz. The ideal switching frequency is between 20 kHz and 2 MHz. The output voltage is regulated by the duty cycle of the switch. When the S1 switch is switched on, the current flows through the L1 coil and the S1 switch, and the energy is stored in the magnetic field of the coil. A current does not flow through the D1 diode and the load current is provided via the C1 capacitor. When the S1 switch is switched off, the drop in the L1 coil current is immediately supplied with its back-electromotive force and the L1 coil voltage is added to the source voltage. The current flows through the L1 coil, the D1 diode, and the $R_L$ load, and thereby the capacitor C1 is charged. Therefore, the output voltage is greater than the input voltage and the voltage equation is as follows:

$$V_{out} / V_{in} = 1 / (1 - D), \tag{6}$$

where $V_{out}$, $V_{in}$, and $D$ are the output voltage, the input voltage, and the duty cycle, respectively. The $1 - D$ value is proportional to the on position time of the S1 switch. The boost rate is as follows:

$$V_{out} / V_{in} = T / T_{off}, \tag{7}$$

where $T$ is the switching cycle (s) and $T_{off}$ is the off cycle of switching (s).

## 2.3. P&O MPPT principle

The power obtained from TEGs varies by not only load variations but also temperature differences. This results in a change in MPP. In this case, a MPPT algorithm is used to monitor the MPP. MPPT is realized by changing the $D$ value of the S1 switch in the boost converter. This is explained for MPPT in Figure 2a.

For better understanding of the MPPT principle in TEGs, it is assumed that the voltage/power curve in Figure 2a first starts at point A. The target is the capture of T, which is the MPP. The voltage at point A is V2 and power is P5. If the voltage value is increased from V2 to V3, the power value will be from P5 to P6. The new operating point on the power curve is C. Again, when the voltage value is reduced from V2 to V1 while at point A, the power value also comes from P5 to P3. The operating point is D in the power curve, which is a sign of a drop in the power value. Accordingly, in order to reach T from A, the voltage will need to be increased continuously. In other words, the voltage value must be increased in order to capture the MPP in the region where the derivative of the power is positive according to the voltage. On the other hand, given point B, the variation in voltage and power will be different. If the voltage is reduced and brought from V5 to V4, the power value also comes from P2 to P4. The new operating point is E, which is an increase in the power value. However, if the voltage value is increased from V5 to V6 at point B, the power value comes from P2 to P1 and the power value is reduced. Accordingly, the new operating point on the power curve is F. In other words, the voltage value must be reduced in order to capture the MPP in the region where the derivative of the power is negative according to the voltage. These possibilities are given in Table 1.

The P&O MPPT algorithm, which needs to be composed to operate the system at the MPP point, is shown for the boost converter in Figure 2b. Firstly, the current and voltage values are measured by sensors. Secondly, the power value is calculated. The changes in the power and voltage are found and then the change value in power is queried. If the power change is positive, the voltage change is questioned and if it is positive, $D$ value is reduced by $\Delta D$. If the voltage change is negative, $D$ value is increased by $\Delta D$. Then it is returned to the beginning again. With a new measurement, the power value is calculated and the new power and voltage variations are found. According to these values, if the power change is negative, the voltage change is again questioned. If the voltage change is positive, $D$ value is increased by $\Delta D$. If the voltage change is negative, $D$ value is reduced by $\Delta D$. This process is continued until the MPP value.
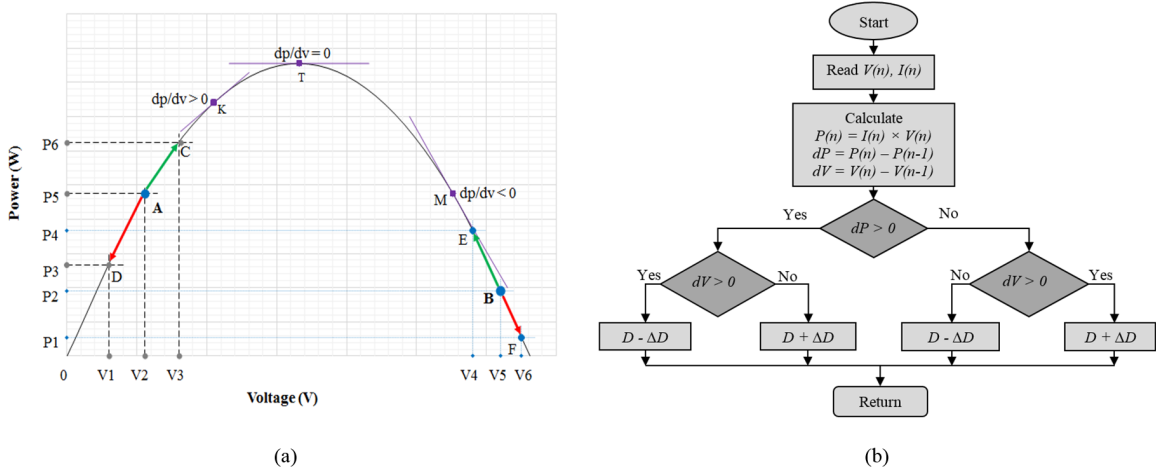


**Figure 2**. For MPPT principle (a) voltage/power curve of TEG and (b) P&O algorithm.

**Table 1**. P&O MPPT algorithm probabilities.

| Voltage variation $\Delta D$ | Power variation $\Delta P$ | Direction of P&O MPPT |
|---|---|---|
| + | + | + |
| + | − | − |
| − | + | − |
| − | − | + |

Although the MPP point in the P&O algorithm can be found, oscillations occur around the point because the process is still running at the point. This is a disadvantage and it is desirable to minimize these oscillations. Large $\Delta D$ values result in bigger oscillations in the MPP, although this results in rapid MPP capture. Moreover, although small $\Delta D$ ranges result in slow MPP capture, this reduces the magnitude of MPP oscillations. Another drawback is that the MPP will change when the temperature difference changes and in this case a separate oscillation will occur for the presence of the new MPP.
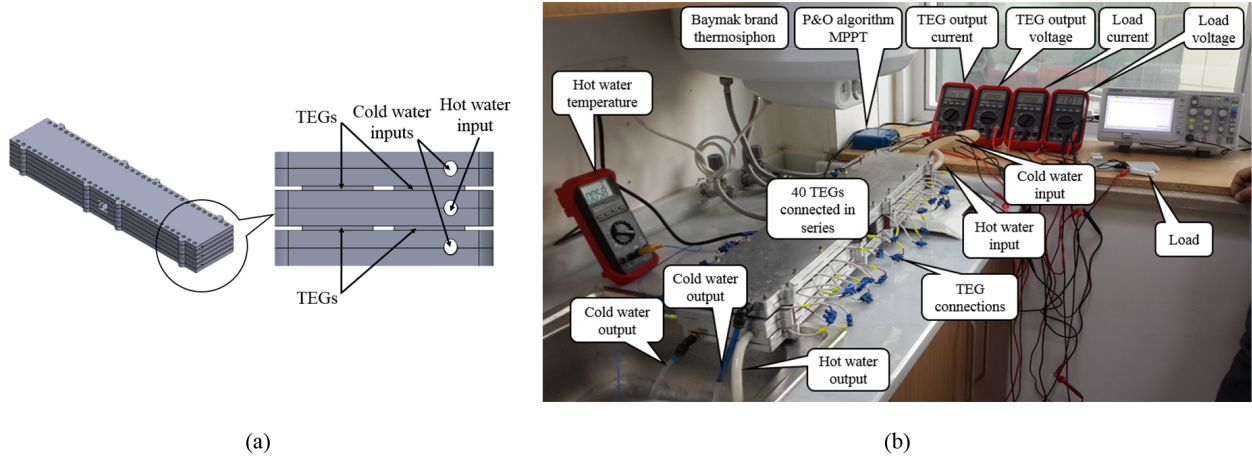
### 2.4. Experimental setup

When a TEG is used alone in a system as a single module, the obtained power value is low. To increase this power value, they should be connected in series or parallel. For this purpose, a hot/cold plates design was prepared as shown in Figure 3a. A setup of 40 TEGs was used in the setup. Those were placed between three aluminum plates. Twenty of them were connected in series in order to increase the voltage value. Additionally, in order to enhance the current value, these two groups of 20 were connected in parallel. In the experimental installation, hot and cold water were passed from the middle and outside aluminum plates, respectively, for providing the temperature difference. Thus, electric energy was generated by the obtained temperature difference.

In order to compare the simulation with the experimental results, the experimental setup given in Figure 3b was carried out. In Figure 3b, five Brymen BM 907S digital measuring instruments were used. The input/output current/voltage values of the TEG system were measured by four of them. The current and voltage measurement error values of the measuring instruments were 1.2% and 0.6%, respectively. With the help of another measuring device, both the hot and cold water outlet temperature values of the TEG system were taken. The measurement error value of the measuring instrument was 0.4%. A K-type point thermocouple was used to measure the temperature values. As a hot water input source in the system, a Baymak brand thermosiphon was preferred. The device increased the water temperature to about 90 °C. The temperature value of the hot water was taken from the temperature indicator on the thermosiphon. The measurement error value of this was 0.5%. For the cold water inlet of the system, running water was used. Four stone resistors were used to see the system output power values depending on load changes. During the experiments, the flow rates of the hot and cold water entering the TEG system were kept constant and they were taken out via the wash basin after use.

### 3. Method

In this section, the modeling of TEGs with Seebeck coefficient and temperature values given the datasheets of manufacturers, the TEG modeling in series and parallel without MPPT, and the TEG modeling in series and parallel with a P&O MPPT boost converter by means of MATLAB/Simulink are explained.

**Figure 3**. TEG (a) hot/cold plates design and (b) experimental setup.

## 3.1. TEG modeling with MATLAB/Simulink

In the present study, the TEGs manufactured by TES Thermoelectric Systems were utilized. Their properties are given in Table 2.

**Table 2**. TEG properties.

| Properties | Value |
|---|---|
| Hot surface temperature, $T_h$ | 250 °C |
| Cold surface temperature, $T_c$ | 30 °C |
| Open circuit voltage, $V_{OC}$ | $4 \pm 0.4$ |
| Short circuit current, $I_{SC}$ | $5.8 \pm 0.6$ |
| Load matching resistance, $R_{in} = R_L$ | 0.7 Ω |
| Load matching output voltage | $2.0 \pm 0.2$ |
| Load matching output current | $2.9 \pm 0.3$ |
| Load matching output power $R_{in} = R_L$ | 5.8 W |
| Seebeck coefficient | 185 $\mu$V/K |
| Figure of merit | $2.86 \times 10^{-3} \mathrm{K}^{-1}$ |
| ZT | 0.8 |

Modeling of a TEG modeled and simulated through MATLAB/Simulink is shown as a temperature-dependent voltage source in Figure 4. In the modeling, the TEG output power was obtained by Seebeck coefficient and hot/cold side temperatures. In Figure 4a, one TEG was used. The temperature difference was calculated in the modeling. Moreover, the internal resistance value was entered in the modeling as shown Figure 4b. Here the TEG modeling is a temperature-dependent controlled voltage source.

## 3.2. TEG modeling in series and parallel without MPPT

Increasing the power generated from TEGs is carried out by series and parallel connection of the TEGs. The modeling of TEGs connected in series and parallel is depicted in Figure 5. The number of connected modules
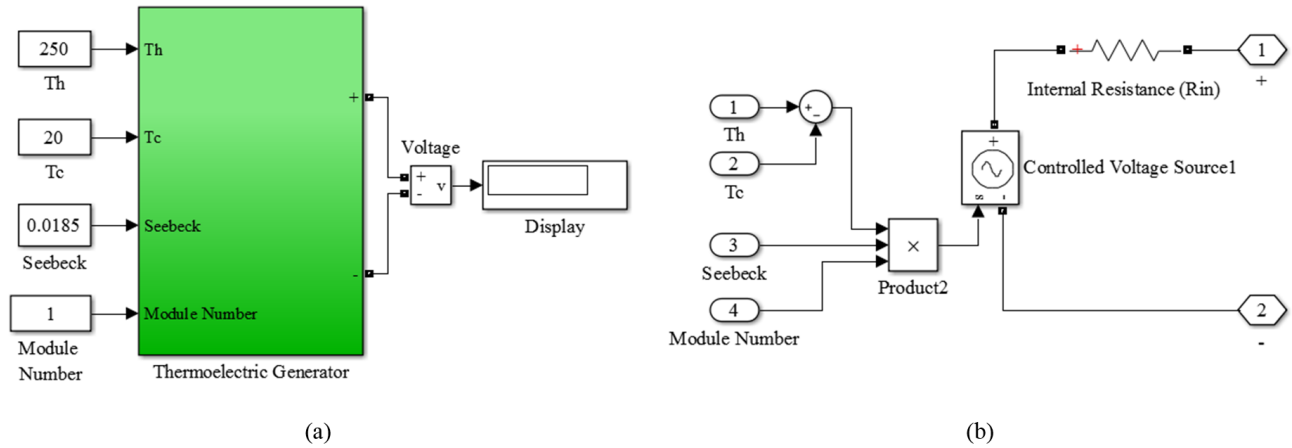
(a)   (b)

**Figure 4**. For one TEG, (a) modeling and (b) internal structure.

in the TEG modeling was 20 in series. In this case, the internal resistance of this model was $0.7 \times 20 = 14\ \Omega$. In order to increase the generated power, a separate model consisting of 20 TEGs was added to the series connected model in parallel. Thus, the TEG internal resistance value of the system was $14/2 = 7\ \Omega$. In addition, current, voltage, and power indicators were put to measure the power to be generated depending on load and temperature variations.
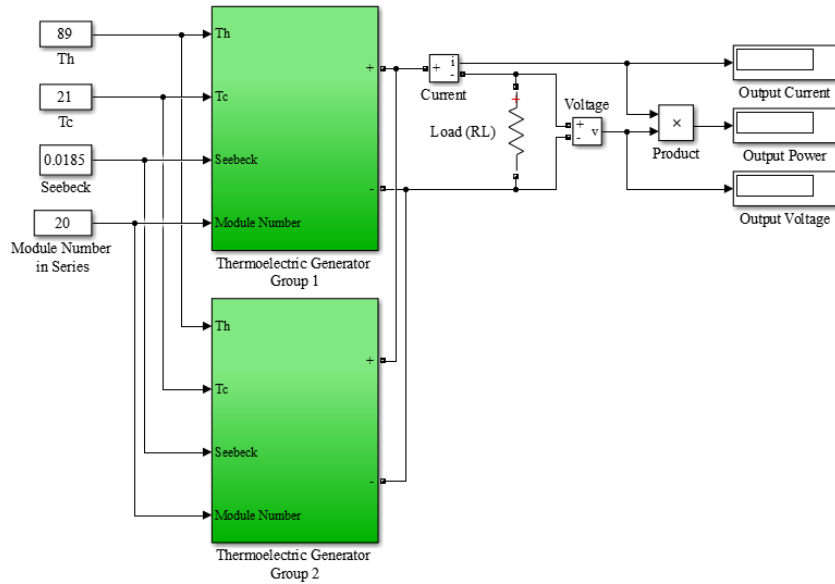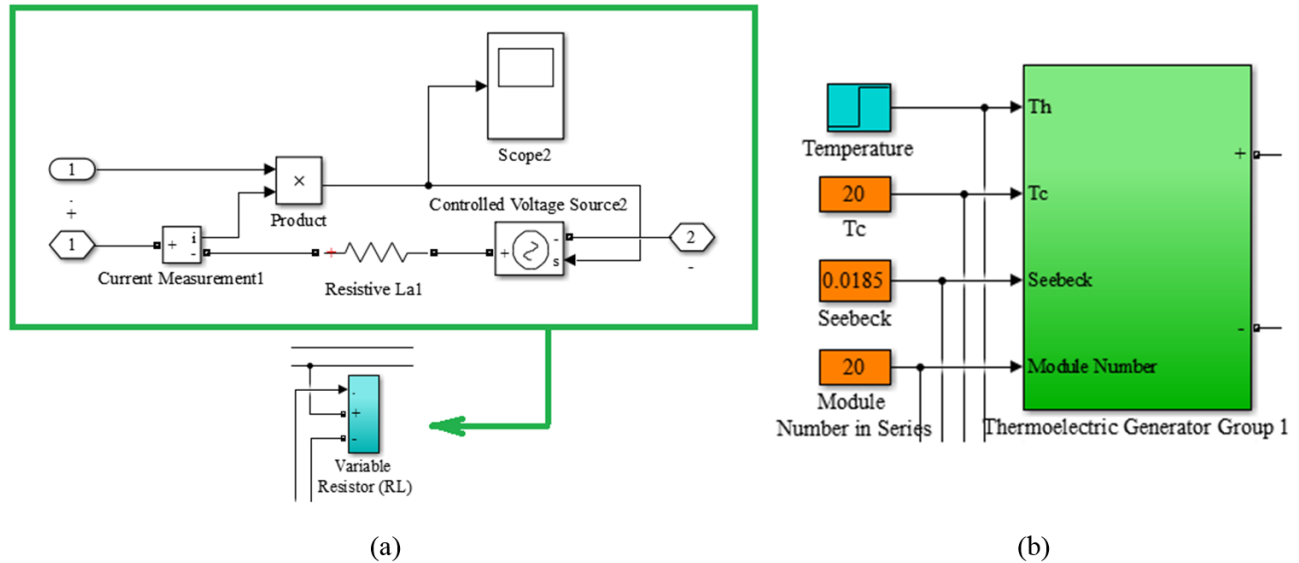


**Figure 5**. TEG modeling in series and parallel.

## 3.3. TEG modeling in series and parallel with a P&O MPPT boost converter

A boost converter with P&O MPPT was included in the designed modeling as shown in Figure 6. Its parameter values were selected as L1 = 1 mH, C1 = 3000 $\mu$F, and switching frequency f = 20 kHz. The power variations generated from the TEG system in series and parallel were minimized by the modeling.

131
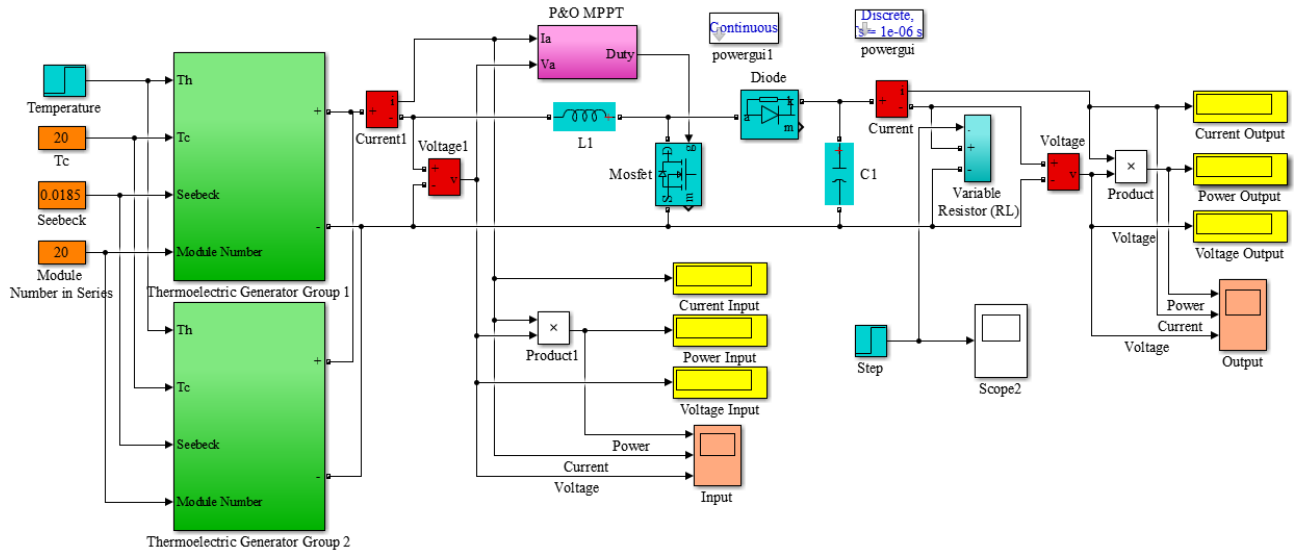
**Figure 6**. TEG system modeling with a P&O MPPT boost converter.

In Figure 6, a variable resistor was connected to the boost converter output. That was changed to determine the MPPT of the boost converter at different load variations. In addition, a variable temperature signal was applied to the hot side input in order to determine the reaction of the boost converter with P&O MPPT at different temperatures. The modeling of the variable resistor and the variable temperature signals are detailed in Figure 7.



(a)
(b)

**Figure 7**. Structure of (a) variable resistor and (b) variable hot side temperature.

In Figure 7, for determining the value of MPPT, the current, voltage, and power indicators were connected to both the TEG output and the output of the boost converter with P&O MPPT. Lastly, two oscilloscopes were put to measure the time responses of both the TEG output and the boost converter with P&O MPPT.

## 4. Results and discussion

Here the results and evaluations obtained from the TEG modeling and the experimental setup are presented in three stages. Firstly, the results and evaluations of the TEG modeling in series and parallel without MPPT are given. Then the results and evaluations of the TEG modeling in series and parallel of the boost converter with P&O MPPT are explained. Lastly, the experimental verification of the simulated system is presented.

### 4.1. Results and evaluations of the TEG modeling in series and parallel without MPPT

The results were taken from Figure 5. First, temperatures were kept constant and a variable load was connected directly to the TEG output terminals. The hot side temperature was entered as $250 °C$ depending on the given datasheet information. In addition, the cold side temperature was $20 °C$. The variable load was also gradually increased from 1 Ω to 200 Ω in eleven steps. Depending on the variable load values, the obtained voltage/power curve without MPPT is given in Figure 8a.

In Figure 8a, the red line marked with rounded pointers indicates the power without MPPT. When the load value was 7 Ω, the highest power was obtained from the TEG because the value was that of load matching. There was a decrease in the obtained power under and above that. On account of the fact that it moved away from the impedance matching, the generated power decreased. Finally, the lowest generated power was obtained for the load value of 200 Ω.

In order to measure the variable temperature response, the load resistance was kept constant as 7 Ω, which was an MPP point. Then the hot side temperature was changed. In that situation, the cold side temperature was fixed at 20 °C. The hot side temperature was gradually increased from 30 °C to 250 °C in ten steps. The results obtained are given in Figure 8b.
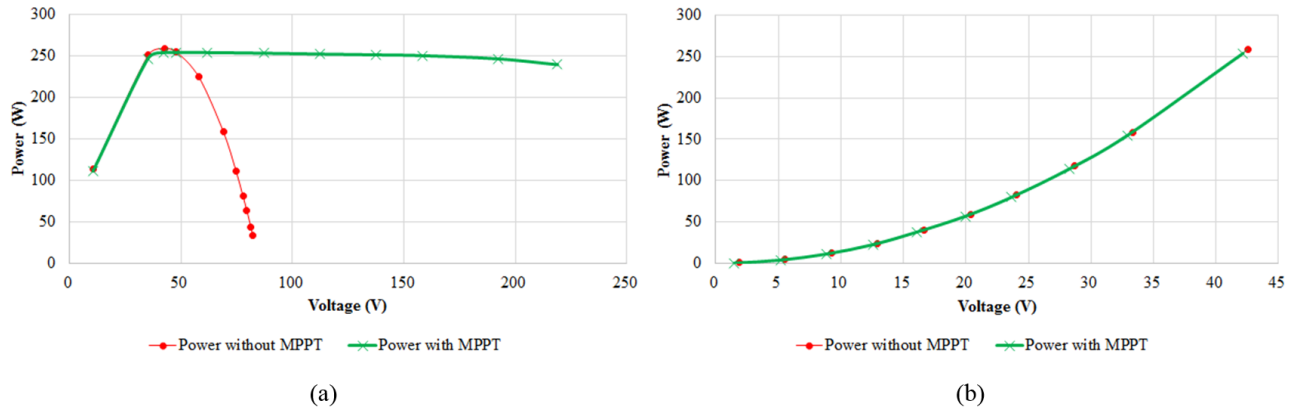


**Figure 8**. Results of the TEG modeling connected in series and parallel without MPPT as a function of (a) the variable load values and (b) the variable temperature values.

In Figure 8b, the red line marked with rounded pointers illustrates the power without MPPT taken as a function of hot side variable temperature values. When the temperature values were taken into consideration, it was seen that an increase in the temperature difference was very effective at the generated power value. The values may not be possible when considering the generation of electrical energy from waste heat in geothermal areas through the help of TEGs. However, it is possible to achieve a temperature difference of 100 °C in these geothermal fields. In such an area, according to the simulation results, power of about 30 W could be obtained from a system of 40 TEGs connected to a load resistance of 7 Ω. The change in temperature results in a change

in the internal resistance of TEGs, because when the hot side temperature rises, the internal resistance of TEGs increases. In that case, the MPP point shifts.

## 4.2. Results and discussion of the TEG modeling of the boost converter with P&O MPPT

The obtained results in the modeling were taken from the modeling shown in Figure 6. First, temperatures were kept constant and the load resistance was changed. The output data of both the TEG output and the boost converter with P&O MPPT are shown in Table 3. For each value, the simulation was run for 1 s. Furthermore, the percentage values were illustrated for how much MPPT could be monitored for the different load values. After that, the temperature of the hot surface was changed gradually. The cold side temperature and the load resistance values were fixed at 20 °C and 7 Ω, respectively.

**Table 3**. Results of the TEG modeling with a P&O MPPT boost converter as a function of variable load.

| Surface temperatures (°C) | | Load (Ω) $R_L$ | Current (A) $I$ | | Voltage (V) $V$ | | Power (W) $P$ | | MPPT (%) |
|---|---|---|---|---|---|---|---|---|---|
| $T_h$ | $T_c$ | | Input | Output | Input | Output | Input | Output | |
| | | 1 | 10.540 | 10.540 | 11.34 | 10.54 | 119.5 | 111.09 | 92.95 |
| | | 5 | 7.025 | 7.025 | 35.91 | 35.12 | 252.3 | 246.72 | 97.80 |
| | | 7 | 6.055 | 6.021 | 42.72 | 42.15 | 258.7 | 253.79 | 98.11 |
| | | 9 | 6.301 | 5.313 | 40.99 | 47.82 | 258.3 | 254.07 | 98.37 |
| | | 15 | 6.488 | 4.115 | 39.69 | 61.73 | 257.5 | 254.02 | 98.64 |
| 250 | 20 | 30 | 6.056 | 2.905 | 42.72 | 87.16 | 258.7 | 253.20 | 97.87 |
| | | 50 | 5.818 | 2.246 | 44.37 | 112.30 | 258.1 | 252.23 | 97.71 |
| | | 75 | 5.673 | 1.830 | 45.39 | 137.30 | 257.5 | 251.26 | 97.58 |
| | | 100 | 5.567 | 1.582 | 46.13 | 158.20 | 256.8 | 250.27 | 97.46 |
| | | 150 | 5.452 | 1.282 | 46.93 | 192.20 | 255.9 | 246.40 | 96.30 |
| | | 200 | 5.351 | 1.094 | 47.64 | 218.90 | 254.9 | 239.48 | 93.94 |

Table 3 shows that almost all of the generated power of the TEG could be transferred to the output through MPPT, even without impedance matching. It was determined that the highest performance of MPPT was achieved for 15 Ω. Although the power transfer was 253.79 W when the impedance matching of the system was 7 Ω, the value was 254.02 W for 15 Ω with the highest power transfer. In order to compare the power with MPPT and without MPPT, the obtained power and voltage variations are shown in Figure 8a. Here the green line marked with a green cross marker indicates the power with MPPT as a function of load variations. In the system without MPPT, while the power value dropped after 7 Ω impedance matching value, there was no decrease in the system with MPPT.

The results obtained from the output of the TEG and the boost converter with P&O MPPT are detailed in Table 4 when the hot side temperature is changed by keeping the load resistance constant at 7 Ω.

Depending on the data in Table 4, it was seen that the power values obtained in small temperature differences were sufficient for very low power electronic devices. However, in the case of the bigger temperature differences, the increase in the power value was very distinct. In addition, although the transfer value of MPPT was lower in small temperature differences, it was higher in larger temperature differences. When keeping the load at 7 Ω, the obtained power values with MPPT and without MPPT as a function of variable temperature

values are shown in Figure 8b. Here the green line marked with a green cross pointer indicates the power with MPPT.

**Table 4**. Results of the TEG modeling with a P&O MPPT boost converter as a function of variable temperature.

| Surface temperatures (°C) | | Load (Ω) $R_L$ | Current (A) $I$ | | Voltage (V) $V$ | | Power (W) $P$ | | MPPT (%) |
|---|---|---|---|---|---|---|---|---|---|
| $T_h$ | $T_c$ | | Input | Output | Input | Output | Input | Output | |
| 30 | | | 0.282 | 0.213 | 1.725 | 1.490 | 0.486 | 0.317 | 65.24 |
| 50 | | | 0.806 | 0.738 | 5.460 | 5.163 | 4.401 | 3.810 | 86.58 |
| 70 | | | 1.313 | 1.265 | 9.310 | 8.858 | 12.224 | 11.205 | 91.67 |
| 90 | | | 1.850 | 1.790 | 13.06 | 12.55 | 24.161 | 22.465 | 92.98 |
| 110 | 20 | 7 | 2.490 | 2.345 | 15.87 | 16.05 | 39.516 | 37.637 | 95.24 |
| 130 | | | 2.910 | 2.850 | 20.32 | 19.95 | 59.131 | 56.858 | 96.15 |
| 150 | | | 3.416 | 3.379 | 24.19 | 23.65 | 82.633 | 79.913 | 96.71 |
| 175 | | | 4.069 | 4.039 | 28.87 | 28.28 | 117.472 | 114.223 | 97.23 |
| 200 | | | 4.749 | 4.700 | 33.36 | 32.90 | 158.427 | 154.630 | 97.60 |

On the other hand, as another part of the study, the load and temperature variations of the TEG system that have the boost converter with P&O MPPT were recorded depending on time. The modeling was subjected to both load and temperature variations and the MPP values were measured. The system response to the load variations is given in Figure 9a. The system modeling was run at 25 Ω for 0.25 s and then the load resistance was raised to 100 Ω with a large change in the resistance. In that case, the hot side temperature was 250 °C and the cold side temperature was 20 °C.

In Figure 9a, when the TEG system with MPPT was operated with a load of 25 Ω, the time to find the MPP was 0.2 s. When the load value was raised from 25 Ω to 100 Ω, the MPP point was captured in 0.65 s. The values were shown with the help of lines 1 and 2. The increase in load value was very effective at the time of capturing the MPP of the TEG.

On the other hand, the response of the modeling to temperature variation is shown in Figure 9b. The modeling was run for the hot side temperature of 120 °C for up to 0.3 s. After that, the hot side temperature value was raised to the highest utilization temperature of 250 °C suddenly. When the hot side temperature was increased from 120 °C to 250 °C, the time stabilize of the MPP is indicated between lines 1 and 2.

In Figure 9b, the hot side temperature change was suddenly carried out. Although the situation was not seen in real systems, it was effective to measure the system response. When the system was operated with the first 100 °C temperature difference, the MPP capturing time value was less than 0.1 s. Again, when the 230 °C temperature difference occurred, the MPP capturing time value was greater than 0.1 s. When they were evaluated, the MPP capturing time was slightly longer for the high temperature difference value.

## 4.3. The experimental verification results of the simulated system

Firstly, as in the MATLAB/Simulink design shown in Figure 5, the load resistance was directly connected to the TEG terminals and the results were obtained from the experimental setup. Then, as shown in Figure 6, the results of the boost converter with P&O MPPT were taken from the experimental setup. The internal resistance of the TEG system was 7 Ω. During the experiments, the data were recorded for the highest hot side

temperature value of 89 °C and the lowest cold side temperature of 21 °C, which gave maximum/minimum hot/cold sides temperature values. In the experiments, because of the obtained low temperature difference $\Delta T$ = 68 °C, the generated power was about 20 W. Simulation results were obtained for the values. After that, they were compared with the simulation results. Eight different values were used for the connected load of the system, i.e. 1, 5, 7, 9, 15, 30, 50, and 75 $\Omega$.
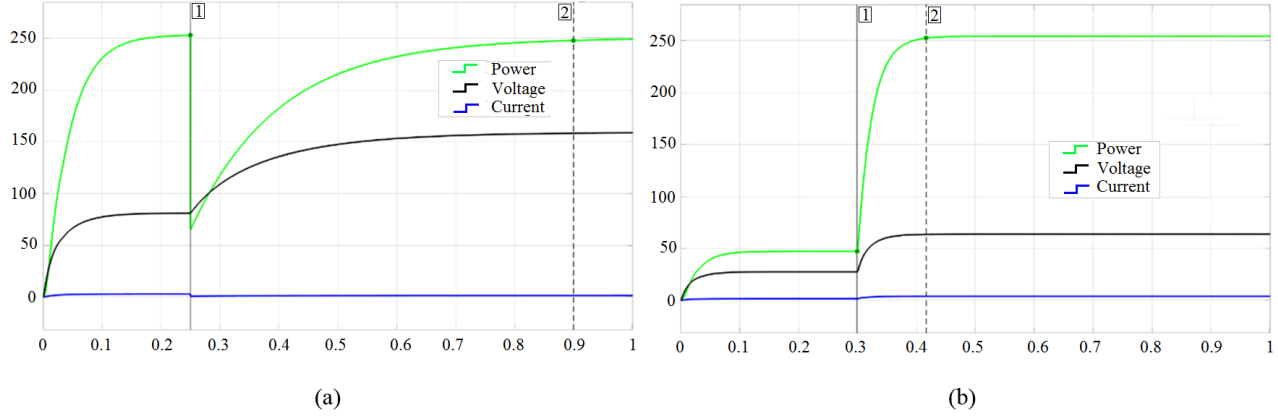


**Figure 9**. Response of the P&O MPPT boost converter to (a) the load resistance and (b) temperature variations.

In the experiments fulfilled without MPPT, the TEG system was highly affected by load changes and the highest power was achieved with the load value about 7 $\Omega$, which was the impedance matching value as expected. The power absolute error values were 0.13, 0.36, and 0.17 when loads of 1, 7, and 75 $\Omega$ were connected, respectively. The comparison of experimental and simulation results without MPPT is shown in Figure 10a as a function of the load variations.

The experimental and the simulation results having the P&O MPPT algorithm embedded in the boost converter are compared in Figure 10b. The obtained power in the application with MPPT was not affected very much by the load variations and the power was close to the impedance matching. The load variations were applied at the steps of 1, 5, 7, 9, 15, 30, 50, and 75 $\Omega$, as in the system without MPPT. According to the obtained results, the power absolute error values between the experimental and simulation results were 0.05, 0.37, and 0.81 for 1, 7, and 75 $\Omega$ loads, respectively.
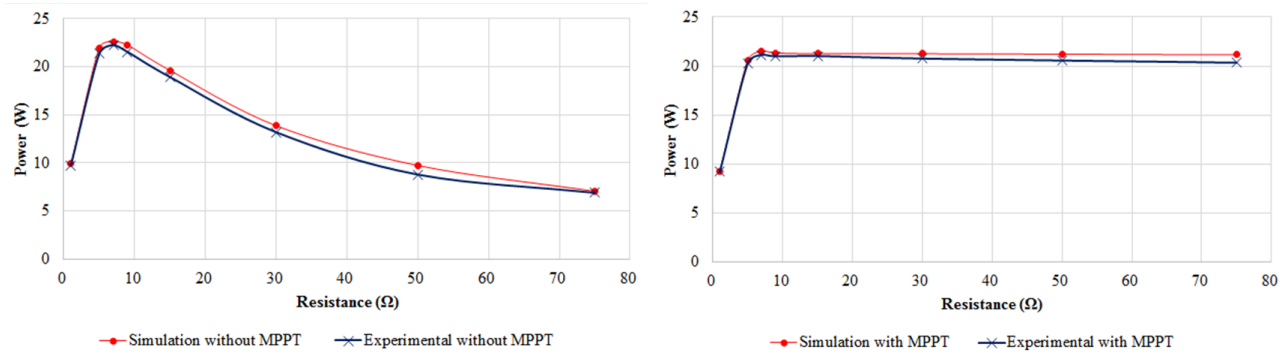


**Figure 10**. Comparison of the power curves as a function of the load variations (a) without MPPT and (b) with MPPT.

## 5. Conclusion

In this study, the modeling of TEGs via MATLAB/Simulink was presented depending on the Seebeck coefficient and temperature values provided by TEG manufacturers. The modeling was designed in such a way that the quantities of TEGs connected in series and parallel could be entered. In addition, both the direct load connection and the load connection with the P&O MPPT boost converter models were carried out to emphasize the importance of impedance matching between the load and TEG internal resistance. Although the modeling without P&O MPPT obtained the highest power on the impedance matching, the highest value was far from this power value for other load values. Furthermore, 98.54% of the TEG power was transferred to the output by means of the proposed boost converter with P&O MPPT. The proposed TEG and P&O MPPT boost converter models were confirmed by means of an experimental liquid–liquid TEG system setup. Consequently, both the TEG and the P&O MPPT boost converter models were presented for TEG users.

## Authors' contributions
H.M. provided the idea, and H.M. and Y.Ç. carried out the simulations and experiments.

## References

[1] Mamur H, Ahiska, R. A review: thermoelectric generators in renewable energy. International Journal of Renewable Energy Research (IJRER) 2014; 4 (1): 128-136.

[2] Champier D. Thermoelectric generators: a review of applications. Energy Conversion and Management 2017; 140: 167-181. doi: 10.1016/j.enconman.2017.02.070

[3] Yavuz AH. Design of a fuzzy logic controlled thermoelectric brain hypothermia system. Turkish Journal of Electrical Engineering & Computer Sciences 2016; 24 (6): 4984-4994. doi: 10.3906/elk-1405-137

[4] Ahiska R. New method for investigation of dynamic parameters of thermoelectric modules. Turkish Journal of Electrical Engineering & Computer Sciences 2007; 15 (1): 51-65.

[5] Omer G, Yavuz AH, Ahiska R. Heat pipes thermoelectric solar collectors for energy applications. International Journal of Hydrogen Energy 2017; 42 (12): 8310-8313. doi: 10.1016/j.ijhydene.2017.01.132

[6] Jagadish PR, Khalid M, Li LP, Hajibeigy MT, Amin N et al. Cost effective thermoelectric composites from recycled carbon fibre: from waste to energy. Journal of Cleaner Production 2018; 195: 1015-1025. doi: 10.1016/j.jclepro.2018.05.238

[7] Mamur H, Ahiska R. Application of a DC–DC boost converter with maximum power point tracking for low power thermoelectric generators. Energy Conversion and Management 2015; 97: 265-272. doi: 10.1016/j.enconman.2015.03.068

[8] Liu YH, Chiu YH, Huang JW, Wang SC. A novel maximum power point tracker for thermoelectric generation system. Renewable Energy 2016; 97: 306-318. doi: 10.1016/j.renene.2016.05.001

[9] Twaha S, Zhu J, Yan Y, Li B, Huang K. Performance analysis of thermoelectric generator using dc-dc converter with incremental conductance based maximum power point tracking. Energy for Sustainable Development 2017; 37: 86-98. doi: 10.1016/j.esd.2017.01.003

[10] Quan R, Zhou W, Yang G, Quan S, A hybrid maximum power point tracking method for automobile exhaust thermoelectric generator. Journal of Electronic Materials 2017; 46 (5): 2676-2683. doi: 10.1007/s11664-016-4875-9

[11] Montecucco A, Knox A. Maximum power point tracking converter based on the open-circuit voltage method for thermoelectric generators. IEEE Transactions on Power Electronics 2015; 30 (2): 828-839. doi: 10.1109/TPEL.2014.2313294

[12] Zainal NA, Yusoff AR, Apen A. Integrated cooling systems and maximum power point tracking of fuzzy logic controller for improving photovoltaic performances. Measurement 2019; 131: 100-108. doi: 10.1016/j.measurement.2018.08.056

[13] Basha CHH, Rani C, Odofin S. A review on non-isolated inductor coupled DC-DC converter for photovoltaic grid-connected applications. International Journal of Renewable Energy Research (IJRER) 2017; 7 (4): 1570-1585.

[14] Kwan TH, Wu X. Maximum power point tracking using a variable antecedent fuzzy logic controller. Solar Energy 2016; 137: 189-200. doi: 10.1016/j.solener.2016.08.008

[15] Husain MA, Tariq A, Hameed S, Arif MSB, Jain A. Comparative assessment of maximum power point tracking procedures for photovoltaic systems. Green Energy & Environment 2017; 2 (1): 5-17. doi: 10.1016/j.gee.2016.11.001

[16] Ezinwanne O, Zhongwen F, Zhijun L. Energy performance and cost comparison of MPPT techniques for photovoltaics and other applications. Energy Procedia 2017; 107: 297-303. doi: 10.1016/j.egypro.2016.12.156

[17] Heidari M. Improving efficiency of photovoltaic system by using neural network MPPT and predictive control of converter. International Journal of Renewable Energy Research (IJRER) 2016; 6 (4): 1524-1529.

[18] Zhang X, Chau KT. An automotive thermoelectric–photovoltaic hybrid energy system using maximum power point tracking. Energy Conversion and Management 2011; 52 (1): 641-647. doi: 10.1016/j.enconman.2010.07.041

[19] Dalala Z, Saadeh O, Bdour M, Zahid Z. A new maximum power point tracking (MPPT) algorithm for thermoelectric generators with reduced voltage sensors count control. Energies 2018; 11 (7): 1-16. doi: 10.3390/en1107182

[20] Liu C, Chen P, Li K. A 500 W low-temperature thermoelectric generator: design and experimental study. International Journal of Hydrogen Energy 2014; 39 (28): 15497-15505. doi: 10.1016/j.ijhydene.2014.07.163

[21] Wu SJ, Wang S, Yang CJ, Xie KR. Energy management for thermoelectric generators based on maximum power point and load power tracking. Energy Conversion and Management 2018; 177: 55-63. doi: 10.1016/j.enconman.2018.09.040

[22] Tsai HL, Lin JM. Model building and simulation of thermoelectric module using Matlab/Simulink. Journal of Electronic Materials 2010; 39 (9): 2105-2111. doi: 10.1007/s11664-009-0994-x

[23] Man EA, Sera D, Mathe L, Schaltz E, Rosendahl L. Dynamic performance of maximum power point trackers in TEG systems under rapidly changing temperature conditions. Journal of Electronic Materials 2016; 45 (3): 1309-1315. doi: 10.1007/s11664-015-4015-y

[24] Montecucco A, Siviter J, Knox AR. The effect of temperature mismatch on thermoelectric generators electrically connected in series and parallel. Applied Energy 2014; 123: 47-54. doi: 10.1016/j.apenergy.2014.02.030

[25] Babu C, Ponnambalam P. The theoretical performance evaluation of hybrid PV-TEG system. Energy Conversion and Management 2018; 173: 450-460. doi: 10.1016/j.enconman.2018.07.104

[26] Irshad K, Habib K, Saidur R, Kareem MW, Saha BB. Study of thermoelectric and photovoltaic facade system for energy efficient building development: a review. Journal of Cleaner Production 2018; 209: 1376-1395. doi: 10.1016/j.jclepro.2018.09.245

[27] Salmi T, Bouzguenda M, Gastli A, Masmoudi A. Matlab/Simulink based modeling of photovoltaic cell. International Journal of Renewable Energy Research (IJRER) 2012; 2 (2): 213-218.

[28] Molina MG, Espejo EJ. Modeling and simulation of grid-connected photovoltaic energy conversion systems. International Journal of Hydrogen Energy 2014; 39 (16): 8702-8707. doi: 10.1016/j.ijhydene.2013.12.048

[29]  Mohammed SS, Devaraj D, Ahamed TI. Modeling, simulation and analysis of photovoltaic modules under partially shaded conditions. Indian Journal of Science and Technology 2016; 9 (16): 1-8. doi: 10.17485/ijst/2016/v9i16/92751

[30]  Abbasoğlu S, Babatunde AA. Evaluation of field data and simulation results of a photovoltaic system in countries with high solar radiation. Turkish Journal of Electrical Engineering & Computer Sciences 2015; 23 (6): 1608-1618. doi: 10.3906/elk-1402-313

[31]  Bellia H, Youcef R, Fatima M. A detailed modeling of photovoltaic module using MATLAB. NRIAG Journal of Astronomy and Geophysics 2014; 3 (1): 53-61. doi: 10.1016/j.nrjag.2014.04.001

[32]  Chouder A, Silvestre S, Sadaoui N, Rahmani L. Modeling and simulation of a grid connected PV system based on the evaluation of main PV module parameters. Simulation Modelling Practice and Theory 2012; 20 (1): 46-58. doi: 10.1016/j.simpat.2011.08.011

[33]  Al-Majidi SD, Abbod MF, Al-Raweshidy HS. A novel maximum power point tracking technique based on fuzzy logic for photovoltaic systems. International Journal of Hydrogen Energy 2018; 43 (31): 14158-14171. doi: 10.1016/j.ijhydene.2018.06.002